Results in Engineering 21 (2024) 101840

Contents lists available at ScienceDirect

Results in Engineering

journal homepage: www.sciencedirect.com/journal/results-in-engineering

Assessment of comfort index (CI) based on vibration characteristics in CNG control system development

Suroto Munahar [a,*], Muji Setiyo [b], Madihah Mohd Saudi [c], Azuan Ahmad [c], Alfin Anugrah Dhimas R [d], Muhamad Hardiansyah [d]

[a] Department of Automotive Engineering, Universitas Muhammadiyah Magelang, Jl. Bambang Sugeng km.05, Mertoyudan, Magelang, 56172, Indonesia
[b] Center of Energy for Society and Industry (CESI), Universitas Muhammadiyah Magelang, Jl. Bambang Sugeng km.05 Mertoyudan Magelang, 56172, Indonesia
[c] Cyber Security and Systems (CSS) Research Unit, Faculty of Science & Technology (FST), Universiti Sains Islam Malaysia (USIM), Nilai, Negeri Sembilan, Malaysia
[d] Laboratory of Automotive Engineering, Universitas Muhammadiyah Magelang, Jl. Bambang Sugeng km.05 Mertoyudan Magelang, 56172, Indonesia

ARTICLE INFO

Keywords:
CNG
Comfort
Vibration
Vibration characteristics
Amplitude

ABSTRACT

Compressed Natural Gas (CNG) is an environmentally friendly alternative fuel that is affordable with high octane value. Although numerous preliminary studies have been developed about CNG, none examines engine vibrations on human body comfort. Based on these problems, this research proposes an experimental method to observe engine vibration characteristics in developing a CNG engine control system for human body comfort. In the first test, the vehicle was evaluated at an environmental temperature of 18 °C and air humidity of 98 %. The second method tested it at environmental temperature of 23 °C and air humidity of 73 %. The results of the first method test showed that the machine vibration amplitude on the x-axis decreased from (2.82–2.25 mm) to (0.85–0.82 mm). The Comfort Index (CI) assessment consisted three checks, namely vibration acceleration, vibration frequency and damping. Vibration acceleration was in a cluster close to III with a maximum threshold value of 4 h for engine vibration. Meanwhile, the test results of the second method showed that the vibration amplitude in the x-axis decreased from (2.82–2.35 mm) to (0.85–0.81 mm. The Comfort Index (CI) assessment was close to cluster II with the threshold value maximum limit of 6 h for engine vibration. The decrease in CI in the second test method was because the second test had a higher environmental temperature and lower humidity. The density of the air/CNG significantly influenced the engine speed and vibration acceleration. This research failed to test ignition angles with various positions, lean and rich AFR, or fuel consumption. Therefore, in future research, is needed to consider these variables.

1. Introduction

In recent decades, there was a significant focus on developments in automotive technology aimed at reducing exhaust emissions, improving engine efficiency, achieving fuel savings [1,2], and enhancing overall vehicle comfort [3]. This focus on technological progress arises from ongoing discussions reported in several research regarding critical issues such as global warming, the limited availability of fossil, environmentally friendly, and economically priced fuels options. Despite these discussions, conventional fuels remain the predominant energy source supporting transportation systems, even though its prices continue to exhibit high volatility closely tied to global economic growth. To address these challenges, various measures have been explored, including the development of electric vehicles and alternative energy sources. Electric vehicles show great potential in reducing emissions, but they face significant challenges, including long charging times, the extensive need for charging stations with large capacities, and relatively high costs. To address these issues, another possible approach is the development of alternative fuels as energy substitutes to reduce dependence on fossil fuels [4]. Compressed Natural Gas (CNG) is an alternative fuel with several advantages, including a high octane rating, low emissions, and economical prices, which can be used in vehicles as a single (mono-fuel), dual (bi-fuel), or mixed fuel (dual-fuel). Extensive research has been conducted on CNG, exploring various variables such as comparative performance between its engine control systems and gasoline-fueled types, engine loading, compression ratio comparisons, control systems integrating hydrogen as a fuel source, and the modeling of CNG control systems.

* Corresponding author.
E-mail address: munahar@unimma.ac.id (S. Munahar).

https://doi.org/10.1016/j.rineng.2024.101840
Received 28 September 2023; Received in revised form 19 December 2023; Accepted 26 January 2024
Available online 4 February 2024

Several research has been conducted on the performance of the CNG engine control systems using the Direct Injection (DI) method alongside gasoline [5]. However, this present research is multifaceted, as it examines the emissions generated during the development of these control systems, focusing on stoichiometric Air-Fuel Ratio (AFR) settings and the use of Exhaust Gas Recirculation (EGR). The effects of implementing the control systems using sequential injection methods under varying engine loads have been previously examined [6]. Hosmath [7] studied the influence of compression ratios on the CNG engine performance, while another research focused on the control systems enhanced with the addition of hydrogen as a supplementary fuel [8]. All three research have discussed the practical implementation of the CNG control systems in vehicles. These investigations failed to address a critical aspect, namely the vibrations generated during the development of the control systems. Lather and Dash [9] observed the emissions generated from the integration of hydrogen fuel into CNG-powered engines, a system known as Hydrogen Compressed Natural Gas (HCNG). Simultaneously, other research has focused on the modeling of CNG control systems [10,11]. These modeling efforts aim to predict significant factors such as the achievement of Air to Fuel Ratio (AFR) and the use of common rail injection systems. All three investigations have successfully developed models for control systems. It is important to pinpoint that none of these research endeavor addressed the issue of vibrations generated by the system.

Enhancing driving comfort in CNG-fueled engines leads to a keen focus on addressing the issue of vibrations generated during operations. The research in this domain has explored several significant variables, including the development of clutch dynamics models to understand and moderate the vibrations generated. Additionally, efforts have been made to reduce vibrations in diesel engines, and to investigate the impact of its propagation in vehicles designed with monocogbody. Lei et al. [3], conducted a research on the development of clutch dynamics models related to vibrations generated. This investigation used the developed models to numerically classify engine vibration faults in vehicles. Their findings showed impressive accuracy, with the actual metric errors being less than 1 %, even when a 5 % noise margin was introduced. The research failed to address engine vibrations when CNG fuel was used.

Preliminary research on vibrations includes endeavors aimed at reducing vibrations in diesel engines [12–14]. For instance, Ryu et al. [12] used dynamic models to predict diesel engine vibrations at idle speeds applied to Sport Utility Vehicles (SUVs). The diesel model was verified by comparing computational and experimental results. In addition, Operational Deflection Shape (ODS) was used to analyze SUV components, such as powertrain, radiators, and the vehicle floor under idle engine conditions. Similarly, Velmurugan et al. [13] conducted a research on vibrations in diesel engines, examining variables related to noise levels and emissions at low speeds. Both of investigations incorporated ODS analysis as a vibration detection method during idle engine conditions. Ashok et al. [14], conducted a research on the vibration of a diesel engine that used a fuel mixture comprising 20 % diesel and orange oil. Their research aims to enhance combustion quality by utilizing orange peel oil as an alternative fuel The research aimed to improve combustion quality by using orange peel oil, as an alternative fuel. Another research [15] investigated diesel engines that have adopted Common Rail technology. These four research failed to discuss vibrations in diesel engines at various speeds.

Vibrations are a common occurrence in vehicles equipped with monocoque body technology [16]. Previous research have dedicated their efforts to assessing how these vibrations, generated by the engine, influence vehicles designed with monocoque body structures. However, the vibrations generated within the monocoque body remained within acceptable parameters. It is important to emphasize that this line of research primarily concentrates on understanding the impact of engine vibrations on the monocoque body. This investigation discusses the impact of engine vibrations on the monocoque body, although it failed to address the driving comfort. Another preliminary research attempted to observe vehicle vibrations when operating on the highway [17,18]. This investigation focused on examining the vibrations generated by vehicles crossing the road under simulated and real-world conditions. The numerical simulations were validated using real-world systems. However, these three research failed to detect any significant changes or the impact of vibration on human comfort.

Homogeneous Charge Compression Ignition (HCCI) is a low-pressure compression engine evaluated based on the vibrations it produces [19]. In a research conducted by Hunicz et al. [19], a single-cylinder HCCI engine was examined based on vibrations generated by installing an accelerometer sensor. Another research attempted to evaluate changes in both Heart Rate (HR) and body vibrations of the engine operator. It was designed to determine suitable engine operation methods while considering the psychological load on the operator [20]. Real-time observations were made regarding vibrations generated by electric vehicles and vibrations in the gas generator rotor system, with particular attention paid to both their direction and vibration speed [21–23]. These three research, despite their contributions to the understanding of vibrations in engine operation, failed to explore the relationship between these parameters and driving comfort.

Another research tried to observe the relationship between vibrations and frequency changes that affect the transmission of acceleration to the head [24]. The primary objective of this research was to evaluate how vibrations from acceleration are transmitted to the head, particularly during dynamic squatting. Meanwhile, advancements in computational power and sensing technology, including Machine Learning (ML) and Deep Learning (DL) were used to detect vibrations with remarkable precision [25]. In this specific research, ML and DL were used to evaluate the characteristics of the vibrations generated. None of these two research addressed the implications of vibrations in respect to human body comfort. Vibrations have been a subject of extensive research, comprising various aspects. Some of the observed variables include the development of dynamic coupling models regarding the vibrations generated, its reduction and impact on diesel and HCCI engines, the influence of Heart Rate (HR), and the effect of engine-generated vibrations on vehicles designed with monocogbody construction. On the contrary, comprehensive research has been conducted on CNG engine control systems, covering a wide range of topics. These investigations have explored the performance of control systems using Direct Injection (DI), the implementation of these systems with sequential injection methods, the influence of compression ratios, the integration of hydrogen into CNG, and the modeling of these control systems. Irrespective of these extensive investigations, the research addressing vibrations generated by CNG-fueled engines concerning human body comfort has not been conducted. The present research aims to fill this gap by examining the characteristics of vibrations generated by the development of control systems concerning human body comfort.

2. Method

2.1. Installation of the CNG system

The designed CNG control system comprised two main systems, namely the fuel and electronic control systems. The fuel system consists of a CNG tank with a working pressure of 200 bar (a), high-pressure pipe (b), reducer (c), mixer (d), solenoid or injector and (e), various sensors and flow meter (f). To measure the vibration characteristics of the CNG engine, the system incorporated an accelerometer sensor installed on the engine (1) and inside the cabin (2). It also included an engine speed sensor (3), Digital Analog Converter -DAC module (4), microcontroller (5), and data capture computer (6). In addition, the AFR was monitored through data acquisition using an oxygen sensor (8), a data logger module (9), and a computer (6). The CNG control system installation consists of an engine speed sensor (3), and control unit (g), including tilt sensor (h). The concept design for measuring the vibration characteristics of the CNG control system is shown in Fig. 1.

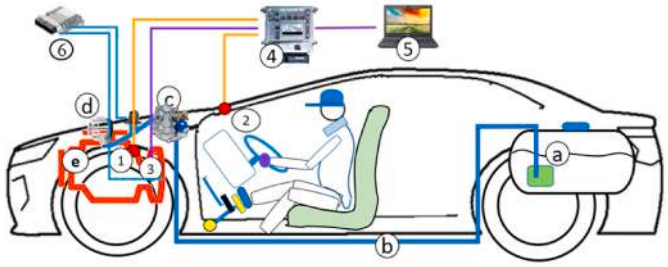

Fig. 1. Concept design for measuring vibration characteristics of CNG control systems.

The setup developed in this research for measuring the characteristics of the CNG control system is showed in Fig. 2.

For reference purposes, engine specifications used in the existing research to examine the dynamics of vibrations generated in CNG vehicles are shown in Table 1.

In this research, multiple software programs were used to design the CNG control system. The C language integrated into the microcontroller (a) within the Arduino software, was designed to create an algorithm for data acquisition. This data acquisition process is essential for recording engine characteristics, forming the basis for developing the CNG control system. MATLAB Simulink is the software used to design CNG control system algorithms (b). The CNG control system incorporated various components such as analog input, signal conditioning, fuzzy logic, and digital output. Analog input 1and 2 are the terminals connected to the crankshaft and road tilt sensors, respectively. In addition, the CNG control algorithm is shown in Fig. 3.) Digital output 1 and 2 are the terminals connected to the CNG injector, and control system, which functions to regulate pulse weight modulation (PWM). PWM serves as a digital domain controller for the CNG injector.

2.2. CNG engine control system

The present research designed a CNG engine control system comprised of a physical, real-scale and a corresponding mathematical model. The primary purpose of the mathematical model was to predict the actual behavior of the real-scale control system. The modeling conditions were validated using data from real-scale experiments. This validation process entailed comparing various datasets, such as engine speed and CNG Air-Fuel Ratio (AFR). In the designed control system, the CNG flow into the engine was regulated by the injectors or solenoids. The designed model was used to describe several operational conditions, including the dynamics of air in the intake manifold, as stated in equation (1).

Table 1
Specifications of the engine used in the research.

Parameter	Specification
Volume engine	1500 cc, Double Overhead Camshaft (DOHC) 16 valves
Fuel type	Gasoline
Cycle	4-stroke
Type of fuel system	Injection
Number of cylinders	4 cylinders, inline
Compression ratio	9.5:1

$$m_a = \frac{V_d \cdot N \cdot \eta_v \cdot \rho_a \cdot}{12 \cdot 10^7} \tag{1}$$

Equations (2) and (3), shows how the control system governs the dynamics of CNG flow into the engine and, consequently, the resulting Air-Fuel Ratio (AFR).

$$m_f = \frac{m_a}{AFR_{st}} \tag{2}$$

$$AFR = \frac{m_a}{m_f} \tag{3}$$

The CNG engine generates torque to propel the vehicle by driving the crankshaft, as stated in Equation (4). Calculating the generated torque comprised several supporting variables, including airflow, AFR, constants, and engine speed [26,27].

$$Torque_{eng} = -181.3 + 379.36 m_a + 21.91 AFR - 0.85 AFR^2 + 0.26\sigma - 0.0028\sigma^2 + 0.027N$$

$$-0.000107N^2 + 0.00048N.\sigma + 2.55\sigma.m_a - 0.05\sigma^2.m_a \tag{4}$$

The airflow within the intake manifold is significantly influenced by the operation of the throttle valve. The airflow dynamics in the CNG engine can be calculated using Equation (5). However, equations (6)–(10), are used to obtain more in-depth exploration of air pressure dynamics.

$$\dot{m}_{ai} = f(\theta).g(P_m) \tag{5}$$

$$f(\theta) = 2.821 - 0.05231\theta + 0.10299\theta^2 - 0.0036\theta^3 \tag{6}$$

$$g(P_m) = 1; if P_m \leq \frac{P_{amb}}{2} \tag{7}$$

$$g(P_m) = \frac{2}{P_{amb}} \sqrt{P_m.P_{amb} - P_m^2}; if \frac{P_{amb}}{2} \leq P_m \leq P_{amb} \tag{8}$$

Fig. 2. Set up for installing equipment for measuring CNG research data.

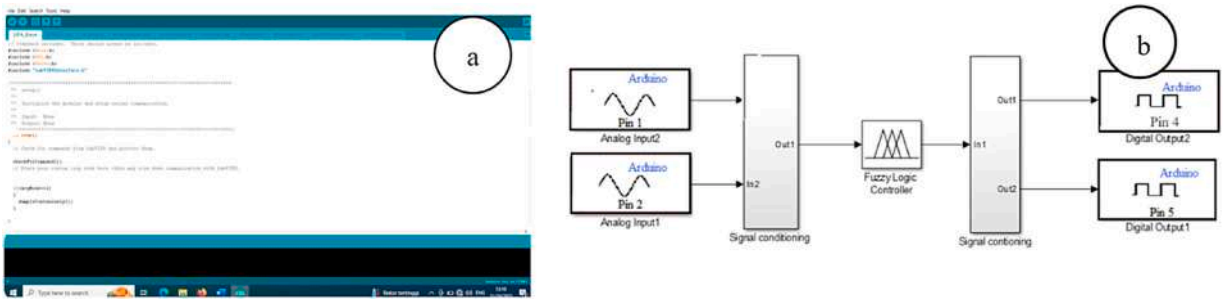

Fig. 3. Programs used in the research were specifically (a) the C language and (b) MATLAB Simulink software.

$$g(P_m) = -\frac{2}{P_{amb}}\sqrt{P_m.P_{amb} - P_{amb}^2}; if P_{amb} \le P_m \le P_{amb} \quad (9)$$

$$g(P_m) = -1; if P_m \ge P_{amb} \quad (10)$$

The movement and change in the speed of air mass and air entering the intake manifold of the engine are determined using equations (11) and (12).

$$\dot{P}_m = \frac{R \cdot T}{V_m}(\dot{m}_{ai} - \dot{m}_{ao}) \quad (11)$$

$$\dot{m}_{mao} = -0.366 + 0.08979N.P_m - 0.0337N.P_m{}^2 + 0.0001N^2.P_m \quad (12)$$

The CNG engine control system model, as presented in equations (1)–(12), was developed through continuous research published in the previous period [11,26].

2.3. Calibration of sensor installation with vibration direction

The CNG engine vibration is measured in two distinct parts, present in the engine and cabin of the vehicle. It also has three directions namely front-back, right-left, and up-down that can be detected by the accelerometer sensor. The calibration of the installed accelerometer sensor on the engine and cabin, including the direction specifications are shown in Table 2. The amplitude value difference between engine and cabin vibrations was evaluated to obtain the dampening capability.

2.4. Assessment of CNG engine vibration characteristics using the comfort index (CI)

To assess human body comfort in relation to the vibration characteristics of the CNG engine, the CI is evaluated based on three significant variables acceleration, frequency, and vibration damping. In addition, the vibration characteristics of CNG engines were compared to that of gasoline.

a Assessment Based on Vibration Acceleration

The vibration acceleration generated by the CNG engine was used to evaluate the characteristics of the resulting ones. It was clustered based on the comfort level of the human body, referring to the safety threshold capability determined in previous research [28]. Muir et al. [28] stated that the acceleration of an object in vibration could affect the human body, and its safety threshold. The unit of acceleration is g, representing the acceleration due to gravity on Earth, which has a value of 1 g = 9,8 m/s^2. This research categorized acceleration into six distinct clusters, as shown in Table 3.

Vibration acceleration is determined by converting the amplitude measured in millimeters (mm), using a data acquisition system. LabVIEW is the data acquisition software used, equipped with an accelerometer sensor. The data acquisition hardware consists of National Instrument 6008 and Atmega, which were connected to the computer. The results of the LabVIEW measured amplitude and acceleration were validated using a vibration meter. Equation (13) was used to convert the amplitude into vibration acceleration in the CNG engine [29,30]. In this equation, A represents the amplitude value in meters, ω is the angular frequency or engine rotational speed in radians per second (rad/s), a denotes vibration acceleration in meters per second squared(m/s^2), and t signifies the assessment time in seconds.

$$a = -A\omega^2 \cdot \sin \cdot \omega t \quad (13)$$

b. Assessment of Vibration Frequency

In addition to measuring the vibration acceleration values to assess ride comfort, the analysis carried out also considers the frequency domain generated by the amplitude of the CNG engine. It is measured in the time domain and converted into that of the frequency for in-depth evaluation. To understand CNG engine vibration, the Fast Fourier Transform (FFT) was used to analyze vibration characteristics in the frequency domain, as expressed in Equation (14), based on previous research [31]. The present investigation used the origin software to design the FFT. $F(\omega)$ and $f(t)$ represents the signals vibration in the frequency and time domain, respectively. $-i\omega$ t is the signal constant value, $-i$ represents the imaginer number, and t denotes the time in seconds. Following this frequency domain analysis, vibrations generated by the CNG engine were assessed based on identifying the safe frequency ranges for the human body [32,33].

$$F(\omega) = \int_{-\infty}^{+\infty} f(t)e^{-i\omega t}dt \quad (14)$$

c. Assessment of Vibration Damping Capability

The amplitude of engine vibrations were evaluated based on their

Table 2
Calibration of accelerometer sensor vibration directions.

No.	Engine Vibration Sensor	Cabin Vibration Sensor	Vibration Direction
1.	Axis X	Axis Y	Front - Back
2.	Axis Y	Axis X	Right - Left
3.	Axis Z	Axis Z	Up - Down

Table 3
Clusters of safety threshold values for the human body regarding the acceptance of vibration acceleration.

No	Cluster	Acceleration Value (±)	Human Body Safety Threshold
1.	I	0,15g (1,47 m/s^2)	16 h
2.	II	0,20g (1,96 m/s^2)	8 h
3.	III	0,30g (2,94 m/s^2)	4 h
4.	IV	0,75g (7,35 m/s^2)	1 h
5.	V	1,25g (12,25 m/s^2)	30 min
6.	VI	2g (19,6 m/s^2)	1 min

damping capabilities, which aims to minimize oscillations in the system [34]. This concept is dependent on the operation of shock absorbers, which functions to reduce the amplitude of oscillations. In practical terms, the lesser the reduction in oscillation, the greater the comfort level experienced by the passengers. Conversely, when oscillations remain more pronounced, the level of comfort tends to diminish.

2.5. Data collection method

Two assessment methods were used to measure the vibration data from the CNG/gasoline engine and cabin. In the first method, measurements were conducted while the vehicle operated at AFR stoichiometry. The engine was set to operate at a medium speed of approximately 2000 rpm, with an ambient temperature of 18 °C. The ignition system was positioned at 5° before the Top Dead Center (TDC), and the air humidity level maintained at 95 %. The second method replicated the conditions of the first, measuring AFR stoichiometry at ±16.5, medium engine speed operated at approximately 2000 rpm, and ignition system positioned at 5° before the TDC. However, there was a difference in ambient temperature, which was 23 °C, while the air humidity remained constant at 73 %. This research used variations in ambient temperature and humidity to assess the entire process.

3. Results and discussion

The design of the CNG control system based on a mathematical model was created using MATLAB Simulink software. To confirm its reliability, the outcomes of the models were validated using real-world experimental data, which included engine speed and AFR measurements. A detailed comparison between the simulation-scale and real-world control systems are shown in Fig. 4. The observed differences between the simulation and real-world scales are not significantly pronounced.

3.1. Assessment of Front-back direction vibration

a. First Method Testing

The front-back direction vibration data from the first testing on the CNG and gasoline engine is shown in Fig. 5(a). The vibrations of this CNG engine showed amplitudes ranging from 2.3 to 2.75 mm. At the 200-s mark, the amplitude was approximately 2.55 mm, corresponding to an engine speed of 2000 rpm. Meanwhile, at the 100-s mark, the amplitude measures approximately 2.43 mm. The frequency obtained at an amplitude of 1.5 mm is 0.01 Hz. Meanwhile, at a signal angle of 300, the frequency ranges from 0 to 0.15 Hz. Gasoline engine vibrations typically fall within the range of 1.8–2.3 mm. At the 200 and 100 s marks, the amplitude measured approximately 2.1 mm, and 2 mm, respectively. The frequency obtained at an amplitude of 1.5 is 0.01 Hz. In addition, when the signal angle is set at zero, the frequency varies within the range of 0–0.25 Hz The front-back direction CNG and gasoline engine vibration data is converted to the frequency domain, as shown in Fig. 5(b).

The dynamics of front-back direction vibrations within the CNG and gasoline vehicle cabin during the first testing phase are shown in Fig. 6 (a). Vibrations in the cabin of this CNG vehicle showed a characteristic amplitude of 0.83 mm at the 100-s mark, occurring when the engine was running at 1850 rpm. Meanwhile, at the 300-s mark, it had an amplitude of 0.836 mm, coinciding at an engine speed of 2050 rpm. The overall amplitude range comprised values ranging from 0.846 to 0.823 mm. In the cabin of a gasoline vehicle, vibrations exhibit a characteristic amplitude of 0.65 mm at the 100-s mark, which corresponds to an engine speed of 2100 rpm. Subsequently, at 300 s the amplitude increases to 0.68 mm, coinciding with an engine speed of 1900 RPM. The total amplitude range for these vibrations falls between 0.65 and 0.69 mm.

The front-back direction cabin vibration was further transformed into the frequency domain using FFT as shown in Fig. 6(b). In this representation, the cabin frequency of a CNG vehicle has a signal angle of −700, comprising frequencies ranging from approximately 0.35 to 0.45 Hz. In addition, an amplitude of 1.5 was associated with a frequency of 0. While a frequency of 0.5 Hz was observed at a signal angle of 0°. The cabin frequency for gasoline vehicles, ranging from 0.25 to 0.5 Hz, has a signal angle of 700. Additionally, a frequency of 0.5 Hz was also observed at a signal angle of 0°.

Data for front-back direction vibration in both the CNG and gasoline engine obtained from the second testing method are shown in Fig. 7(a). These vibrations of this CNG engine showed characteristic amplitudes, with a reading of 2.58 mm observed at a 100-s interval while the engine rotated at 1850 rpm. Furthermore, at the 200-s mark, the amplitude measured 2.68 mm, corresponding to an engine speed of 1900 rpm. The amplitude range for front-back direction vibrations fluctuates between 2.3 and 2.83 mm. This variability is attributed to the oscillation of the engine, which was between 1800 and 2000 rpm, a phenomenon influenced by the higher environmental temperature (23 °C) and 73 % humidity encountered in the second method. Vibrations in the gasoline engine showed lower amplitude, of 2.00 mm observed at 100 s intervals when the engine was running at a speed of 2030 rpm. Furthermore, at the 200 s mark, the amplitude increased to 2.15 mm, corresponding to an engine speed of 2050 rpm. The range of vibration amplitudes in the front-back direction fluctuated between 1.8 and 2.35 mm.

The front-back direction engine vibration data was transformed into a frequency domain using the Fast Fourier Transform (FFT). The resulting frequency representation of the engine behavior is shown in Fig. 7(b). Within this depiction, the CNG engine direction has an amplitude value of 1.5 with a frequency of 0.01 Hz. Meanwhile, as the amplitude approaches 0.1, the corresponding frequency advances 0.5

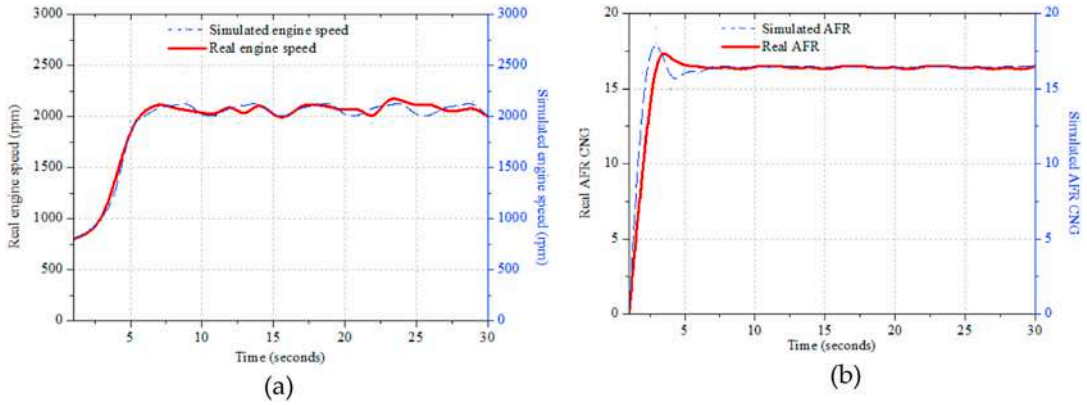

Fig. 4. Comparison of real-scale and simulation engine speed (a) and real-scale and simulation CNG AFR dynamics (b).

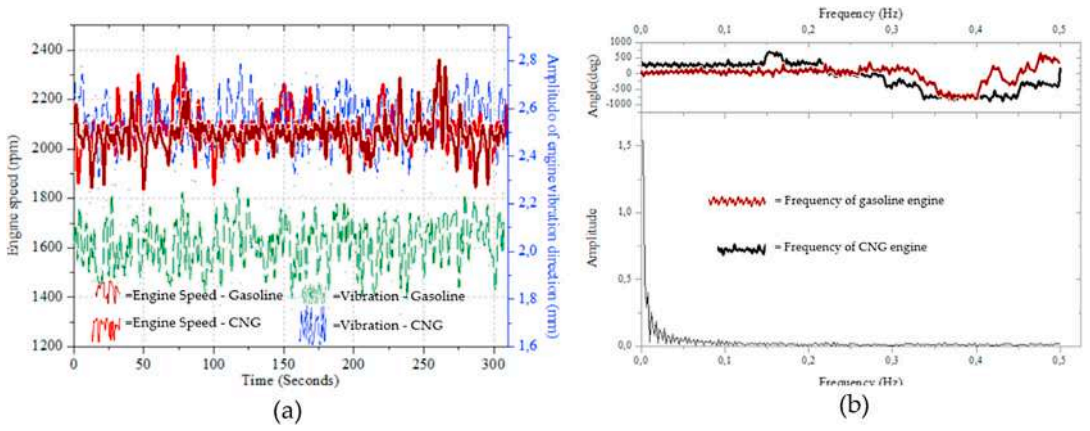

Fig. 5. The vibration direction signal of the CNG and gasoline engine along the x-axis (front-back direction) (a) and frequency domain (b).

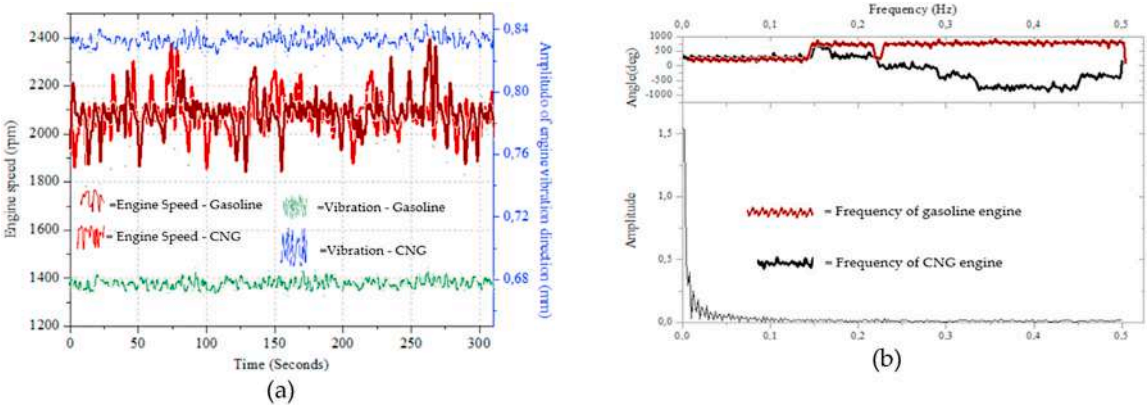

Fig. 6. Vibration direction signal of the CNG and gasoline cabin along the y-axis (front-back direction) (a) and frequency domain (b).

b. Second Method Testing

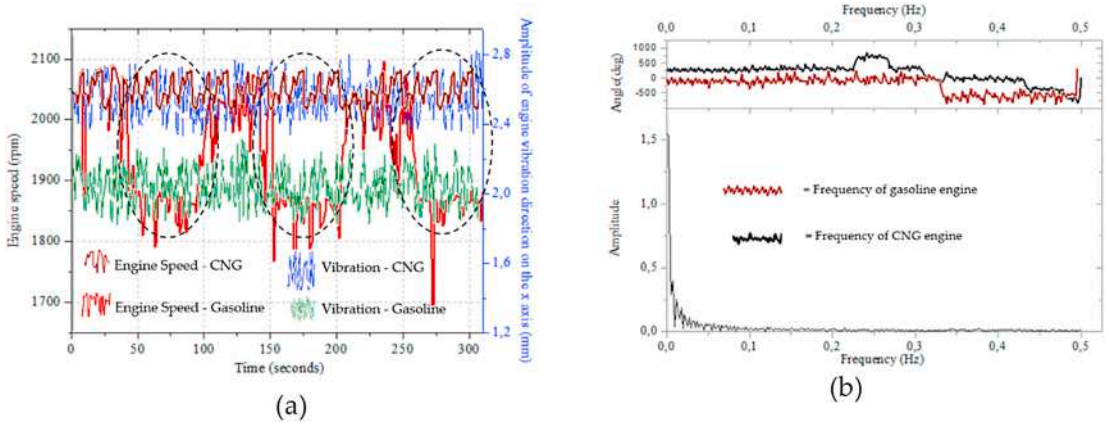

Fig. 7. Vibration direction signal of the CNG and gasoline engine along the x-axis (front-back direction) (a) and frequency domain (b).

Hz. At the signal angle of 200, the frequency nearly reaches 0 tp 0.25 Hz. The gasoline engine has an amplitude of 1.5 and operates at a frequency of 0.1 Hz. As the amplitude approaches 0.1, the corresponding frequency increases by 0.5 Hz. In addition, at a signal angle of −800, the frequency relatively reached 0.5 Hz.

Following the engine assessments, the subsequent step involves measuring vibrations within the cabin. Front-rear direction data in the cabins of CNG and gasoline vehicles is shown in Fig. 8(a). Cabin vibrations in the CNG vehicle show a characteristic amplitude within the range of 0.820–0.845 mm, with a peak amplitude of 0.845 mm recorded at the 90-s mark. The collected data was then transformed into the frequency domain using FFT for further analysis. The resulting frequency domain representation is shown in Fig. 8(b), where a signal angle of 300 corresponds to a frequency range of 0–0.26 Hz. Additionally, a signal angle of 600 is associated with a narrower frequency range of 0.28–0.5 Hz, and it showed an amplitude of 0.05, approaching a frequency of approximately 0.5 Hz. Gasoline vehicle cabin vibrations showed amplitude values ranging from 0.74 to 0.78 mm, with a peak of

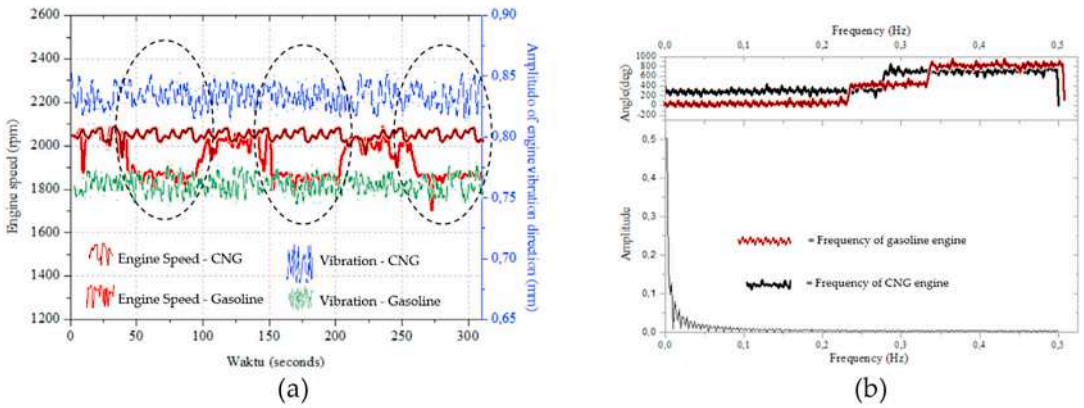

Fig. 8. Vibration direction signal of the CNG and gasoline vehicle cabins along the y-axis (front-back direction) (a) and frequency domain (b).

0.76 mm recorded at the 90-s mark. The signal angle 0 corresponded to a frequency range of 0–0.23 Hz. Additionally, a signal angle of 800 was associated with a smaller frequency range of 0.33–0.5 Hz, with an amplitude of 0.05.

3.2. Assessment of Right - left vibration

a. First Method Testing

Vibrations in both CNG and gasoline engine observed during the first testing method in the right-left direction are shown in Fig. 9(a). The vibrations in the CNG engine showcased a consistent pattern with an amplitude of 2.41 mm recorded at the 100-s mark, corresponding to an engine speed of 1850 rpm. At the 200-s mark, the amplitude was recorded at 2.55 mm, in line with an engine speed of 2050 rpm. Furthermore, the amplitude range for these vibrations is between 2.44 and 2.75 mm. The engine is then transformed into the frequency domain using FFT, as shown in Fig. 9(b). Within this representation, it showed an amplitude of 1.3 mm at 0 Hz. The direction has a signal angle of −500 with a frequency ranging from approximately 0.28 to 0.33 Hz. Vibrations in the gasoline engine had an amplitude of 1.81 mm recorded at the 100-s mark, coinciding with an engine speed of 1850 rpm. At the 200-s mark, the amplitude increased to 1.85 mm, corresponding to an engine speed of 1930 rpm. The amplitude range for these vibrations varies between 1.70 and 1.95 mm. In addition, the frequency obtained at an amplitude of 1.5 was 0.01 Hz, while at signal angle of zero, it ranges from 0 to 0.18 Hz.

The right-left direction vibration data obtained in both the CNG and gasoline vehicle cabins first testing method are shown in Fig. 10(a). However, the vibrations in the CNG engine showed a consistent pattern, with an amplitude of 0.735 mm recorded at the 100-s mark, while coinciding with an engine speed of 1850 rpm. Similarly, at the 200-s mark, the amplitude measures 0.727 mm, corresponding to an engine speed of 2000 rpm. The amplitude range for these cabin vibrations remains within 0.723–0.740 mm. The cabin vibration in the right-left direction were converted to the frequency domain using FFT, as shown in Fig. 10(b). In this representation, an amplitude of 1.6 mm was recorded at 0 Hz. The direction was characterized by a signal angle of 200 with a frequency range of approximately 0–0.22 Hz. Vibrations in the cabin of a gasoline vehicle showed a characteristic amplitude of 0.53 mm at the 100-s mark, coinciding with the engine running at 2100 rpm. Meanwhile, at 300 s the amplitude remained at 0.53 mm, coinciding with an engine speed of 1900 rpm. The general range of amplitude falls within 0.52–0.55 mm.

In the second testing method, the vibration characteristics of the CNG and gasoline engines in the right-left direction are shown in Fig. 11 (a). The vibrations from the CNG engine showed a consistent pattern, with an amplitude of approximately 2.4 mm recorded at the 100-s mark, while coinciding with an engine speed of 1950 rpm. Similarly, at the 200-s mark, the amplitude was recorded at 2.5 mm, in line with an engine speed of 1850 rpm. The amplitude range for these engine vibrations were observed within the narrow range of 2.32 mm–2.80 mm. The cabin vibrations were transformed into the frequency domain using FFT as shown in Fig. 11(b). Within this representation, an amplitude of 1.5 mm was recorded at 0 Hz. The direction is characterized at a signal angle of −600 with a frequency ranging from approximately 0.45 to 0.5 Hz. Conversely, the gasoline engine showed lower an amplitude of 1.80 mm observed at 100 s intervals when the engine was running at 2050 rpm. In addition, at the 200 s mark, the amplitude increased to 1.95 mm, equivalent to an engine speed of 2050 rpm. The range of vibration

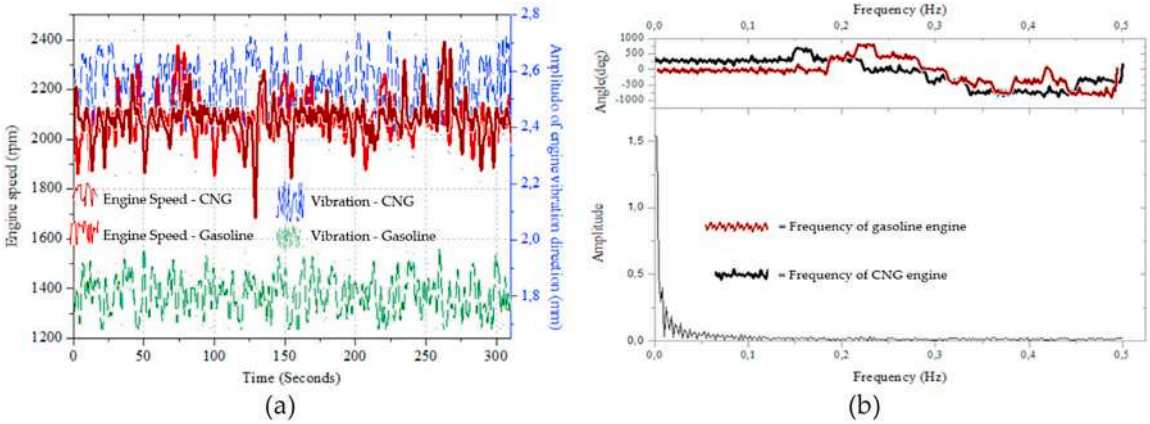

Fig. 9. Vibration direction signal of the CNG and gasoline engine along the y-axis (right-left direction) (a) and frequency domain (b).

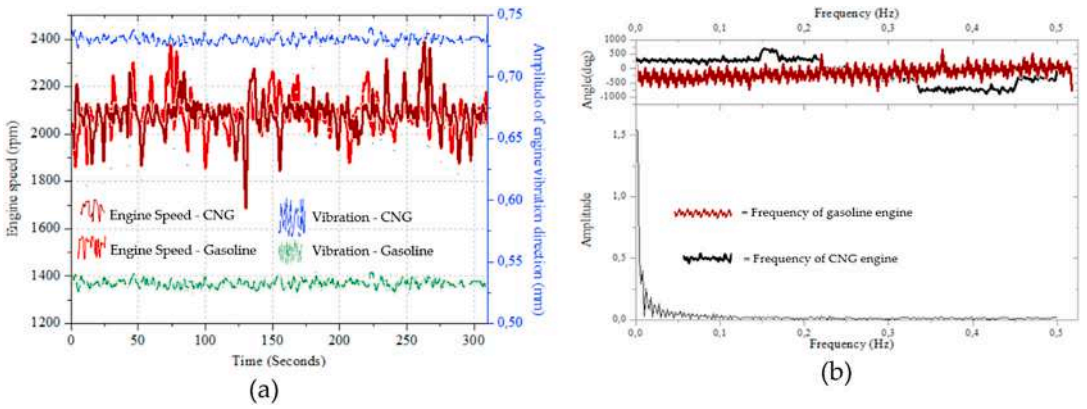

Fig. 10. The vibration direction signals for the cabins of both CNG and gasoline vehicles along the y-axis (right-left direction) (a) and frequency domain (b).

b. Second Method Testing

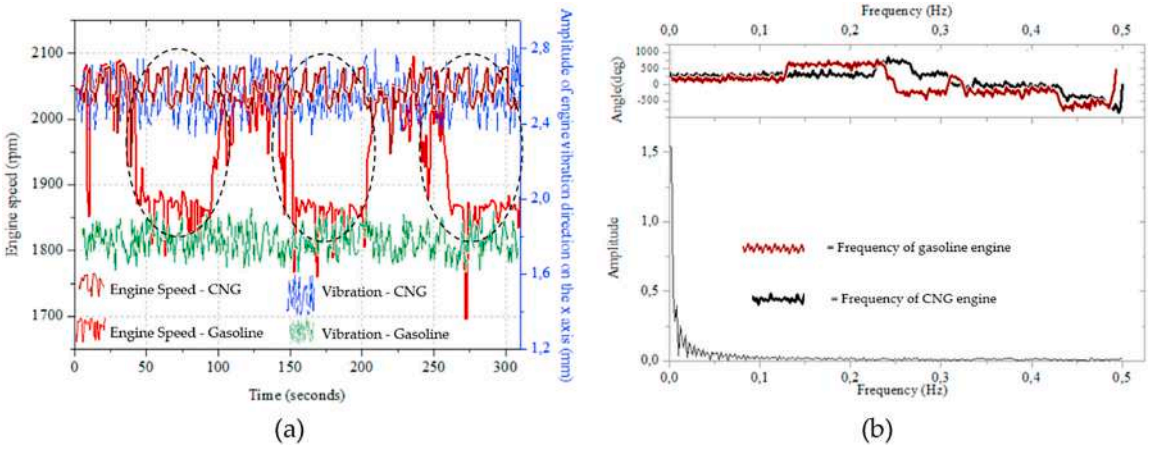

Fig. 11. Vibration direction signals in both the CNG and gasoline engines along the y-axis (right-left direction) (a) and frequency domain (b).

amplitudes in the front-back direction varied between 1.6 and 2.00 mm.

Data for the right-left direction vibrations during the cabins of both CNG and gasoline vehicles second testing are shown in Fig. 12(a). The vibrations within the CNG vehicle cabin showed characteristic amplitudes, with a measurement of 0.715 mm recorded at the 100-s mark, while coinciding with an engine speed of 1950 rpm. Furthermore, at the 200-s mark, an amplitude of 0.73 mm was recorded, in line with an engine speed of 1850 rpm. The amplitude range for these cabin vibrations falls within 0.718 mm–0.740 mm. The cabin vibrations converted into the frequency domain in the right-left direction are shown in Fig. 12 (b). In this representation, an amplitude of 1.5 mm was recorded at a frequency of 0 Hz. Additionally, the direction was characterized by a signal angle of −500, with a frequency ranging from approximately 0.45 to 0.5 Hz. Within the cabin of the gasoline vehicle, vibrations showed amplitudes ranging from 0.62 to 0.65 mm, with a peak of 0.63 mm recorded at the 90-s mark. When the signal angle was set at 100, it corresponded to a frequency range from 0 to 0.3 Hz. Additionally, at a signal angle of 500, a narrower frequency range of 0.26–0.5 Hz was

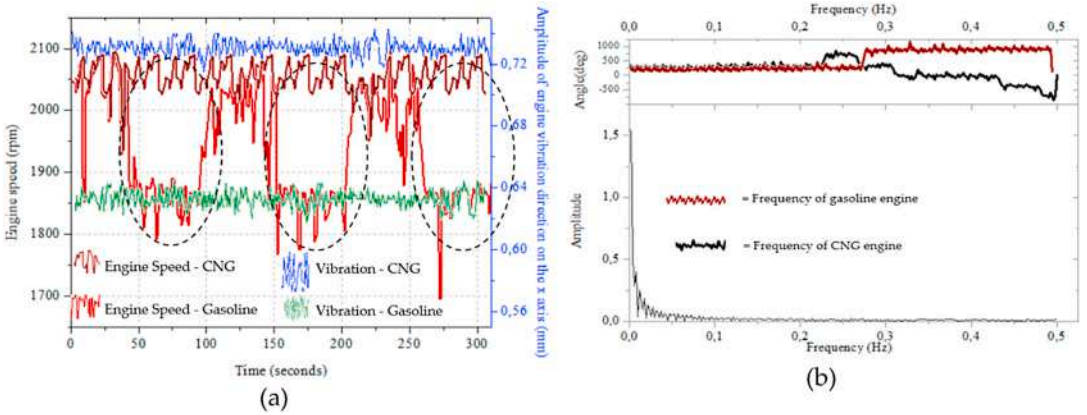

Fig. 12. The vibration direction signal in the cabins of both CNG and gasoline vehicles along the y-axis (right-left direction) (a) and frequency domain (b).

observed at an amplitude of 0.05. This amplitude approached a frequency of approximately 0.01 Hz.

3.3. Assessment of Up-down direction vibration

a. First Method Testing

The engine vibrations in both the CNG and gasoline engines observed in the first testing method, characterized by the up-down direction are shown in Fig. 13(a). The vibrations of the CNG engine consistently recorded an amplitude of approximately 2.60 mm at the 100-s mark, while corresponding to an engine speed of 1850 rpm. Moreover, at the 200-s mark, the amplitude increases to 2.75 mm, in line with an engine speed of 2050 rpm. The amplitude range for these engine vibrations falls within 2.54 mm–2.83 mm. The engine vibrations transformed into the frequency domain, particularly with regard to an up-down direction is shown in Fig. 13(b). In this representation, an amplitude of 1.3 mm was recorded at a frequency of 0 Hz. The direction was characterized by a signal angle of −800 with a frequency ranging from approximately 0.38 to 0.5 Hz. The gasoline engine vibrations showed consistent characteristics, with an amplitude of 2.10 mm recorded at the 100-s mark, corresponding to an engine speed of 2050 rpm. This amplitude increased slightly to 2.20 mm at the 200-s mark, in line with an engine speed of 1900 rpm. The total range of amplitudes for these observations fell between 2.00 and 2.32 mm. A frequency of 0.01 Hz was obtained at an amplitude of 1.5. Meanwhile, at a signal angle of zero, the frequency was within 0–0.08 Hz.

The data for the up-down direction vibrations in the cabins of both CNG and gasoline vehicles second testing are shown in Fig. 14(a). In the cabin of a CNG vehicle, these vibrations showed characteristic amplitudes, with a consistent measurement of 0.96 mm and 2050 rpm, respectively. The amplitude range for these cabin vibrations fell within 0.92 mm–0.95 mm. The cabin vibrations converted into the frequency domain, specifically in the right-left direction are shown in Fig. 14(b). In this representation, an amplitude of 1.4 mm was recorded at a frequency of 0 Hz. This direction was also characterized by a signal angle of - 1000, with a frequency ranging from approximately 0.38 to 0.5 Hz. For gasoline vehicle cabin vibrations, the amplitudes ranged from 0.73 to 0.78 mm, with a peak of 0.75 mm recorded at the 90-s mark. A signal angle of 200 corresponded to a frequency range of 0–0.35 Hz. Additionally, at a signal angle of 300, a narrower frequency range within 0.35–0.5 Hz as observed, at an amplitude of 1.

Data from the up-down direction vibrations in both CNG and gasoline engines are shown in Fig. 15(a). The vibrations in the CNG engine showcased an amplitude of 2.65 mm at the 100-s mark, while coinciding with an engine speed of 2200 rpm. Similarly, at the 200-s mark, the amplitude was recorded at 2.71 mm, in line with an engine speed of 1850 rpm. The amplitude range for these engine vibrations were from 2.5 mm to 2.80 mm. These vibrations were converted into the frequency domain using FFT as shown in Fig. 15(b). In this representation, vibrations with an amplitude of 1.3 mm have a frequency of 0.01 Hz, while those with an amplitude of 0.01 mm correspond with a frequency of 0.5 Hz. The signal angle recorded at 200° has a frequency ranging from 0 to 0.25 Hz. Conversely, vibrations in the gasoline engine showed lower amplitudes, with readings of 2.20 mm at 100-s intervals when the engine was running at 2050 rpm. However, at the 200 s mark, the amplitude increased to 2.30 mm, equivalent to an engine speed of 1850 rpm. The amplitude values in the front-back direction were within the range of 2.00–2.35 mm.

The data from the up-down direction vibrations in the cabins of CNG and gasoline vehicles are shown in Fig. 16(a). These characteristics of the CNG vehicle cabin revealed an amplitude of 0.972 mm recorded at the 100-s mark, while coinciding with an engine speed of 2000 rpm. Furthermore, at the 200-s mark, an amplitude of 0.951 mm was recorded, in line with an engine speed of 1850 rpm. This resulted in an amplitude range within 0.94 mm–0.98 mm. The transformation of these vibrations into the frequency domain using the FFT method for further analysis are shown in Fig. 16(b). In this representation, vibrations with an amplitude of 1.3 mm correspond to a frequency of 0.01 Hz, while those with a signal angle of 200 mm were recorded at a frequency of 0–0.28 Hz. The vibrations within the cabin of the gasoline vehicle showed amplitude ranging from 0.82 to 0.88 mm, with a peak of 0.85 mm recorded at the 90-s mark. At a signal angle of −100, these vibrations corresponded to frequency values within the range of 0–0.18 Hz. Additionally, a signal angle of 300 resulted in narrower frequencies within the range of 0.19–0.5 Hz, accompanied by an amplitude of 0.05.

3.4. Assessment of vibration acceleration

a. Assessment of Front-Back Direction

The assessment of engine and cabin vibration acceleration was conducted using the LabVIEW-designed data acquisition, which was validated using a vibration meter. Two distinct methods, discussed in the data acquisition sub-section, are used. In both cases, the conversion of amplitude into acceleration, as validated by using Equation (1). The results for the first and second methods are shown in Figs. 17 and 18.

There are significant differences in the acceleration assessment results between the two methods of CNG and gasoline engines. In the case of the CNG engine, the acceleration in the first method tended to be higher, approaching 3 m/s^2 (0.3 g), while in the second one, its value was approximately 2.5 m/s^2 (0.25 g). However, in the first method, the acceleration value approached 1 m/s^2 (0.1 g), while the second one yielded approximately 0.85 m/s^2. The decrease in acceleration in the

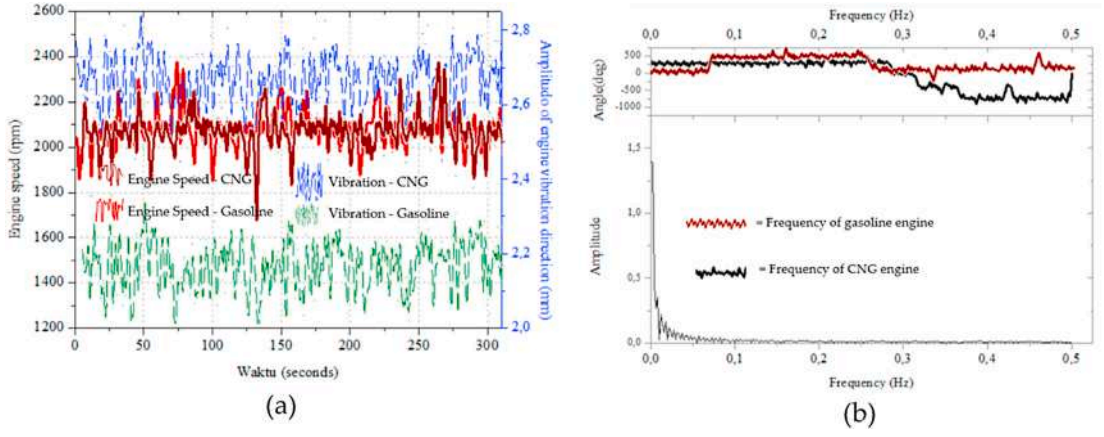

Fig. 13. Vibration direction signal for both the CNG and gasoline engines the z-axis (up-down direction) (a) and frequency domain (b).

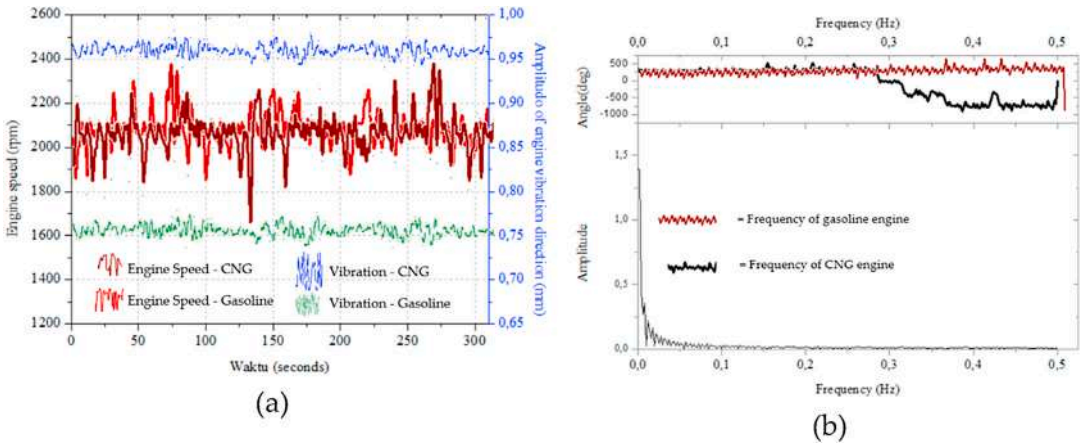

Fig. 14. Vibration Direction Signal in the cabins of both CNG and gasoline vehicles along the z-axis (up-down direction) (a) and frequency domain (b).

b. Second Method Testing

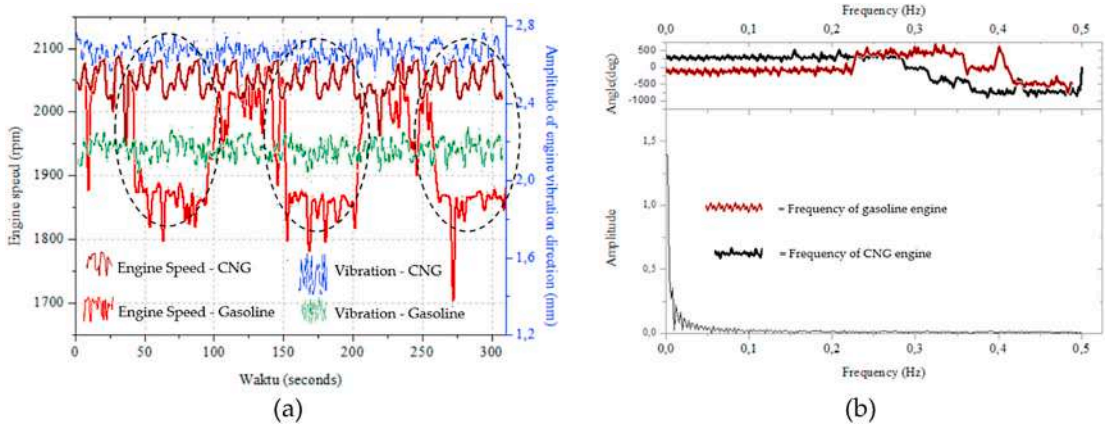

Fig. 15. Vibration direction signals of both the CNG and gasoline engines, specifically focus on the z-axis (up-down direction) (a) and frequency domain (b).

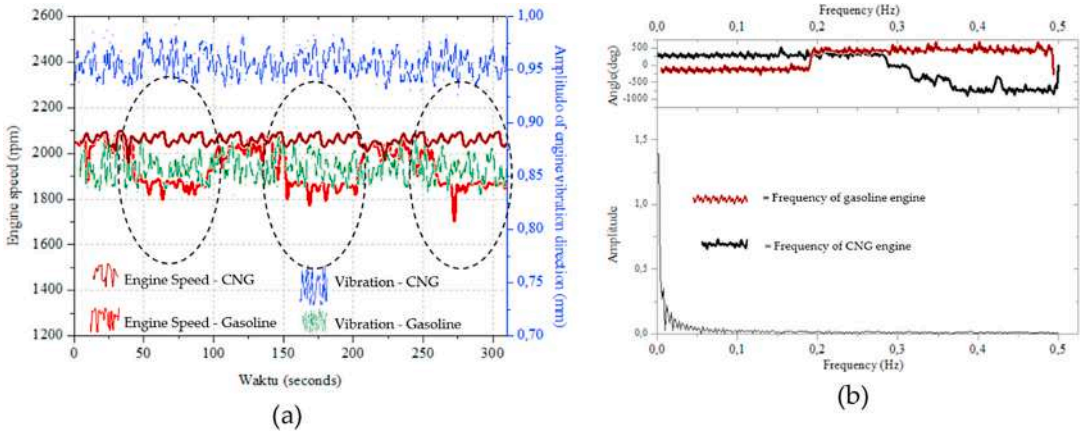

Fig. 16. Vibration direction signal the CNG and gasoline engine the z-axis (up-down direction) (a) and frequency domain (b).

second method was due to the higher temperature and lower environmental humidity. In the case of gasoline engines, the acceleration in the first method was the same as in the second one, ranging from 2 m/s^2 (0.2 g) to 3 m/s2 (0.3 g). However, the cceleration value of a gasoline engine is lower than that of a CNG.

The acceleration dynamics in the right-left direction for both the engine and cabin vibrations, during the first and second methods on the CNG and gasoline engines are shown in Figs. 19 and 20. The acceleration assessments of the CNG engine in the first method tend to be higher, approaching 2.5 m/s^2 (approximately 0.25 g), compared to the second, which recorded a value of 2 m/s^2 (0.2 g). Meanwhile, for the cabin acceleration assessments, the first method, yielded a value of approximately 0.7 m/s^2 (0.07 g), while in the second, it approached 0.3 m/s^2 (0.03 g). In the case of gasoline engines, the acceleration in both the first and second methods were the same, with values ranging from 1 m/s^2 (0.2 g). The acceleration value of a gasoline engine is less than that of a

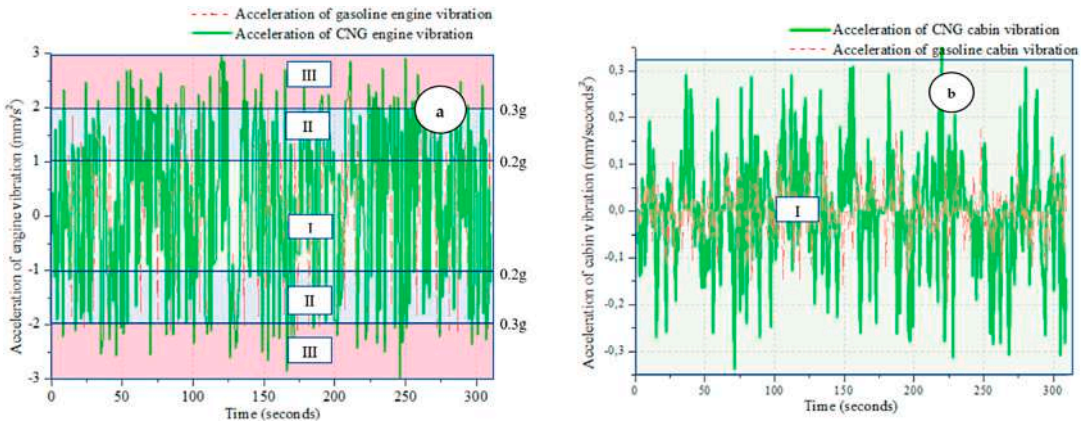

Fig. 17. Acceleration assessments result from engine (a) and cabin (b) of the CNG and gasoline vehicle vibrations in the front-back direction in the first method.

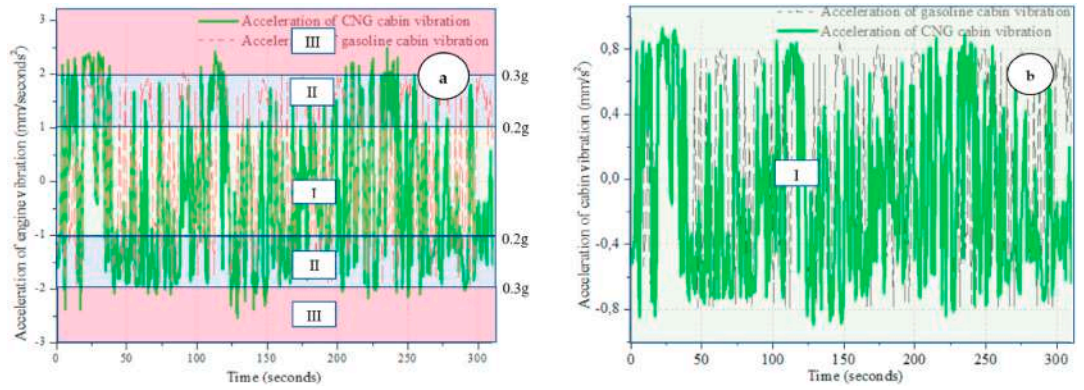

Fig. 18. Acceleration assessments result from the engine (a) and cabin (b) of the CNG and gasoline vehicle vibrations in the front-back direction in the second method.

b. Assessment of Right-Left Direction

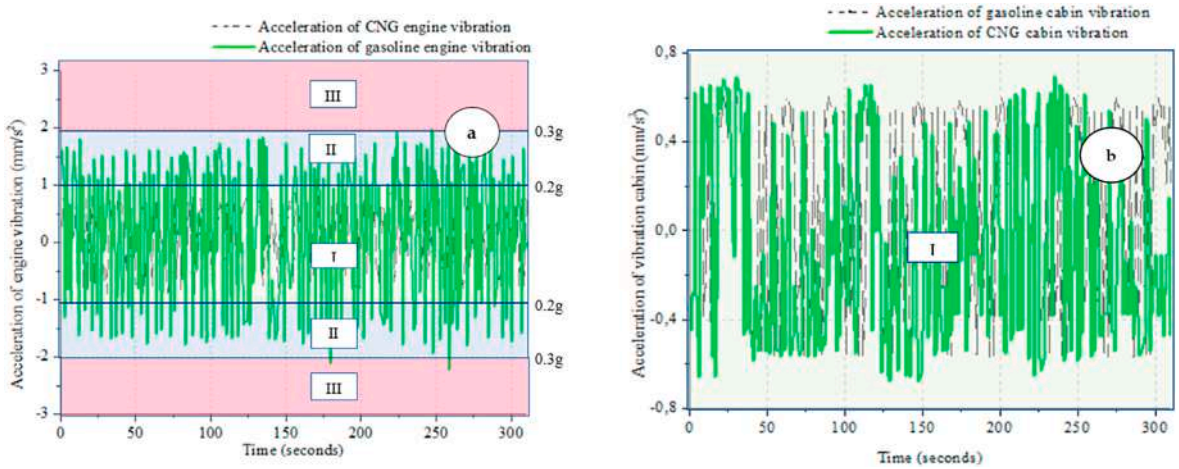

Fig. 19. Acceleration assessment results from engine (a) and cabin (b) of the CNG and gasoline vehicle vibrations in the right-left direction using the first method.

CNG.

Acceleration measurements were conducted for both engine and cabin vibrations in the up-down direction, using the first and second method on both CNG and gasoline engine as shown in Figs. 21 and 22. In the case of CNG engine acceleration, assessments from the first method tend to yield a higher value, relatively 3 m/s^2 (approximately 0.3 g), compared to the second one, which was recorded at 2.5 m/s^2 (approximately 0.25 g). For the assessment of cabin acceleration, using the first and second methods, the values were 1 m/s2 (0.1 g) and 0.98 m/s2 (0.1 g), respectively. In the context of gasoline engines, the acceleration in both the first and second methods tended to similar, typically between 2 m/s^2 (0.2 g) and 3 m/s2 (0.3 g). However, the acceleration value of a gasoline engine is less than that of a CNG.

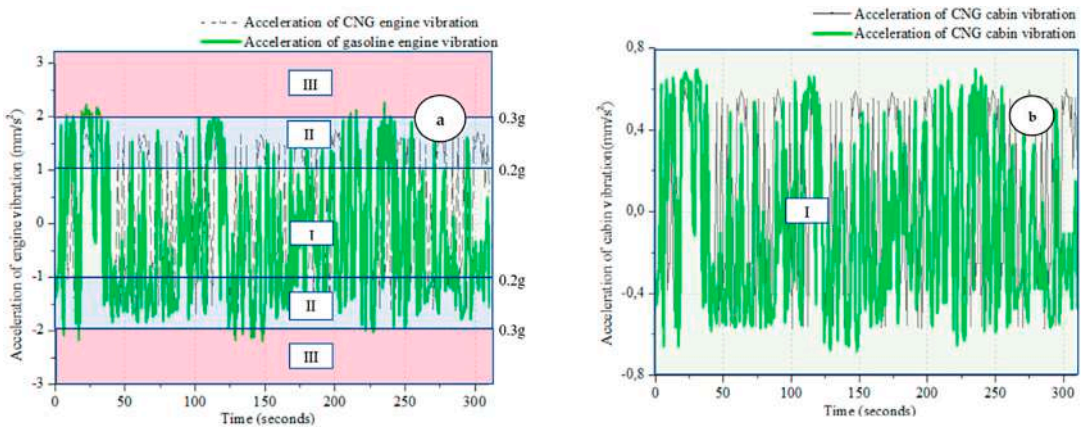

Fig. 20. Acceleration assessment results from engine (a) and cabin (b) of the CNG and gasoline vehicle vibrations in the right-left direction using the second method.

c. Assessment of Up-Down Direction

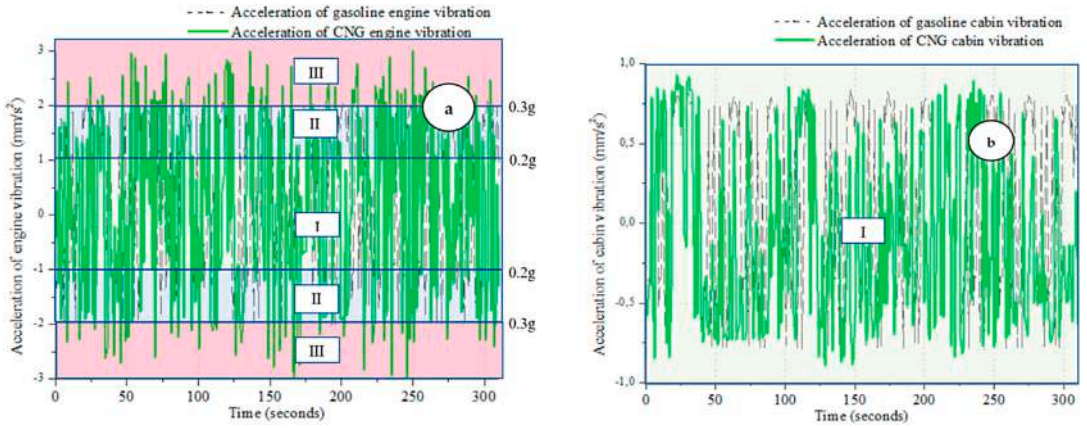

Fig. 21. Acceleration assessments result from engine (a) and cabin (b) of the CNG andgasoline vehicle vibrations in the vertical up-down direction using the first method.

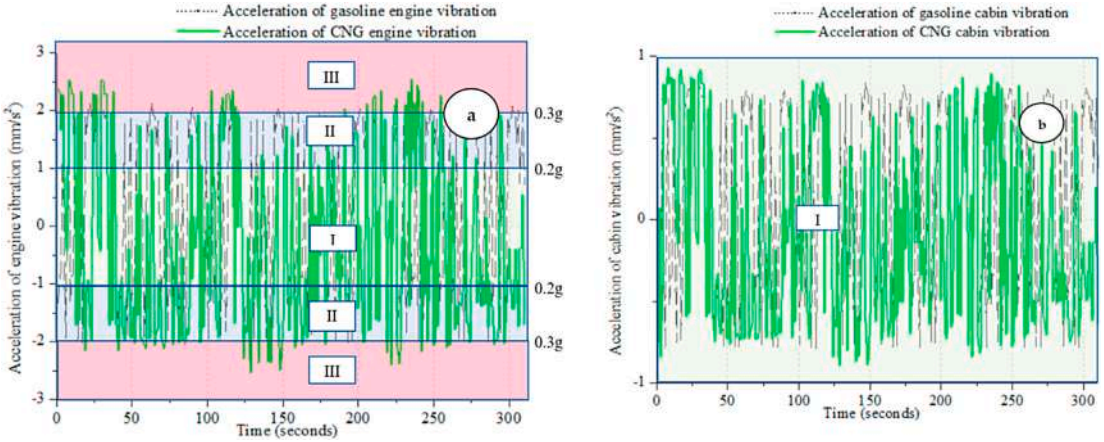

Fig. 22. Acceleration assessments result from engine (a) and cabin (b) of the CNG and gasoline vehicle vibrations in the vertical up-down direction using the second method.

3.5. Discussion

a. Vibration Analysis Based on Acceleration

The acceleration assessments of CNG engine vibration in the front-back, right-left, and up-down directions had different values. The first method yielded a higher acceleration value, of approximately 3 m/s^2 (0.3g), compared to the second one, which was recorded within the range of 2 m/s^2 (0.2g). The first and second methods were categorized under clusters III and II, with a maximum threshold of 4 h and 6 h for engine vibrations, respectively. As for the cabin, both methods fell under cluster I, indicating a longer threshold. These findings suggest that the

CNG engine, operating under lower environmental temperatures and higher humidity conditions, tends to exhibit greater acceleration levels, leading to reduced comfort levels, as observed in the first method. Conversely, the second method indicates that the CNG engine, under higher environmental temperatures and lower humidity, tends to have lesser acceleration levels, resulting in enhanced comfort levels. This research is in line with previous ones that discussed the relationship between vibration acceleration and human comfort [28].

During the acceleration testing, a unique phenomenon was observed in the vibration of both the CNG vehicle engine and cabin. This phenomenon specifically occurred in the second testing method. It is characterized by a periodic rise and fall in the activity of the CNG engine, visually represented by black circles. This phenomenon occurred as follows.

1. The appearance of the black circle in the diagram signifies a notable oscillation in engine speed, mainly triggered by the periodic activation of the radiator fan. This oscillation occurred as the engine experienced varying levels of load due to the intermittent operation of the radiator cooling fan. When the temperature of the engine exceeded the optimal range, it resulted in a decrease in its speed, as the fan engages to provide cooling. Conversely, when the engine temperature drops below the ideal range, the radiator fan ceases its rotation to assist in the cooling process. The rotation of the radiator fan caused the alternator to spin harder because it produces higher electrical power, thereby leading to an increase in the engine load.
2. The periodic oscillation of the engine speed, triggered by the intermittent operation of the radiator fan, is a phenomenon specific to the testing conducted using the second method. In this method, vehicles were tested at high environmental temperatures and lower humidity of approximately 23 °C and 73 %, respectively. However, when vehicle testing was conducted using the first method, under conditions marked by low environmental temperatures and higher air humidity levels of approximately 18 °C and 98 %, the engine speed does not exhibit the same up-and-down pattern, even though the radiator fan operates intermittently.
3. In the second method, where vehicles were tested under high environmental temperatures and lower humidity of approximately 23 °C and 73 %, the air entering the engine experienced a significant reduction in density. This decrease in air density greatly affected the combustion process in the engine, resulting in a decrease in engine power. Conversely, the first method included testing vehicles in conditions with lower environmental temperatures and higher humidity of approximately 18 °C and 98 %, respectively. Under these conditions, the engine showed higher power output even when the radiator fan turns on and off periodically, its speed remained stable.

b. Analysis of Vibration Based on Generated Frequencies

For the assessment of engine and cabin vibrations using the first testing method in the front-back, right-left, and up-down directions, the frequencies obtained were higher compared to the second one. In the first method, vibrations in the front-back direction had frequencies of 0.1 Hz and 0 Hz with amplitudes of 2.8 mm and 600 mm, respectively. Signals at a −400-degree and −700-degree angles showed frequencies ranging from 0.45 to 0.5 Hz, and 0.35–0.45 Hz, respectively. In the second testing method, frequencies ranged from 0.45 to 0.5 Hz at a −500-degree angle and signals at 0° were recorded at frequencies between 0.35 and 0.43 Hz. According to the research by Liu [32] and Zang et al. [33], frequencies less than 2 Hz fall into the nearly imperceptible or uncomfortable category. In this research, the recorded frequency values remained in the range of 0.3–0.5 Hz, which still falls within the comfortable category.

c. Vibration Analysis Based on Damping Ability

The evaluation of vibration and its impact on human body comfort can be assessed based on the ability to dampen oscillation amplitudes. When oscillation amplitudes decrease, comfort levels generally increase, while higher amplitudes tend to reduce comfort. In this research, both the first and second testing methods showed that engine vibrations, in the front-back, right-left, or up-down directions, showed significant damping effects. This was proven by the substantial reduction in oscillation amplitudes observed in the cabin. For instance, in the front-back direction, engine vibrations ranged from 2.82 to 2.25 mm, which decreased to 0.85 to 0.82 mm in the cabin. The damped oscillation amplitudes were as low as 0.27 to 0.03 mm. Likewise, the second method showed significant damping in the front-back direction, with engine vibrations decreasing from 2.82 to 2.35 mm and 0.85 to 0.81 mm in the cabin. This reduction in damped amplitudes, ranging from 0.57 to 0.04 mm, serves as a measurable indicator of human comfort, thereby supporting findings from prior research [34].

d. Verification and Validation

To verify and validate this research by comparing it with previous research. Changes in vibration acceleration, frequency characteristics, and damping ability are a reference to validate this research. Mui et al. [28] study to verify changes in vibration acceleration on driver comfort. Liu [32]and Zhang et al. [33] as verification of vibration characteristics for comfort when driving. Liu et al. [34] research to verify the damping ability of vibration oscillations on driving comfort.

e. Analysis of Engine RPM Towards Humidity

In the first data acquisition method, controlled environmental conditions were maintained, with temperature set at 18 °C and humidity at 98 %. The ignition system was consistently positioned at 5° before Top Dead Center (TDC), and the Air-Fuel Ratio (AFR) for CNG remained at stoichiometry (16.5). Throughout this method, the engine operated within a range of 2000 rpm. In the second method, the environmental temperature was measured at 23 °C with a humidity level of 73 %. Similar to the first method, the ignition system was positioned at 5° before TDC, and the AFR for CNG was maintained at stoichiometry (16.5). The engine was set to operate at a medium speed, however, it could not remain constant. It reduced to 1700 rpm from 40 to 100 s and 150–200 s. The variations in environmental temperature and humidity levels significantly influenced the speed of the CNG engine during the data collection process.

4. Conclusion and recommendation

In conclusion, the vibration characteristics of CNG-fueled vehicle engines in respect to human comfort were evaluated using the Comfort Index (CI), which comprised three assessments. Regarding vibration acceleration, the first method yielded higher acceleration values, approximately 3 m/s^2 (0.3g), compared to the second one, which fell within the range of 2 m/s^2 (0.2g). These findings placed the first and second methods in cluster III, and II where the maximum threshold values for engine vibrations was set at 4 h, and 6 h, respectively. When evaluating CNG engine in terms of vibration damping, it was evident that both the first and second methods effectively dampened oscillations in the front-back direction. This damping was observed through a reduction in oscillation amplitudes. In the case of the first method, amplitudes decreased from a range of (2.82–2.25 mm) to (0.85–0.82 mm), resulting in a dampened amplitude of approximately (0.27–0.03 mm). The findings of this research suggested that CNG-powered vehicle engines produced low-frequency vibrations which were categorized as comfortable. This comfort was attributed to the fact that these vibrations remained below 2 Hz. Considering the three assessment aspects of CNG engines, it was discovered that environmental temperature, and humidity factors greatly influenced the resulting vibrations and human

body comfort. As a result, there was a clear need for further research in this field. The engine settings in this research not yet to account for variations in fuel consumption measurements, adjustments in the AFR from lean to rich, and in ignition timing. Consequently, further research was deemed necessary to enhance the comprehensiveness of this topic.

CRediT authorship contribution statement

Suroto Munahar: Writing – review & editing, Writing – original draft, Visualization, Software, Methodology, Formal analysis, Data curation, Conceptualization. **Muji Setiyo:** Investigation, Formal analysis, Conceptualization. **Madihah Mohd Saudi:** Validation, Formal analysis. **Azuan Ahmad:** Supervision, Investigation. **Muhamad Hardiansyah:** Data curation, Conceptualization.

Declaration of competing interest

The authors declare that they have no known competing financial interests or personal relationships that could have appeared to influence the work reported in this paper.

Data availability

Data will be made available on request.

Acknowledgment

The authors are grateful to BRIN (National Research and Innovation Agency) for funding this research and to LPPM (Institute of Research and Community Service) Universitas Muhammadiyah Magelang, Indonesia for their support during this project.

References

[1] S. Karagiorgis, K. Glover, N. Collings, Control challenges in automotive engine management, Eur. J. Control 13 (2007) 92–104, https://doi.org/10.3166/ejc.13.92-104.
[2] S. Munahar, A. Triwiyatno, J.D. Setiawan, M. Munadi, Assessment of fuel management clusters in the development of a driving behavior control system model using lookup table mapping to improve fuel savings, Results Eng 18 (2023) 101170, https://doi.org/10.1016/j.rineng.2023.101170.
[3] A. Lei, C.X. Song, Y.L. Lei, Y. Fu, S. Zheng, Research on the models of coupling dynamics and damage Classification for vehicle-engine vibration, Math. Probl Eng. 2020 (2020), https://doi.org/10.1155/2020/5907613.
[4] A.R. Noviyanti, Y. Yuliyati, D.R. Eddy, Solihudin, R. Tjokronegoro, Struktur dan Morfologi Elektrolit Apatit Lantanum Silikat Berbahan Dasar Silika sekam padi, J. Mater. Dan Energi Indones. 6 (2016) 1–6.
[5] T. Kar, Z. Zhou, M. Brear, Y. Yang, M. Khosravi, J. Lacey, A comparative study of directly injected , spark ignition engine performance and emissions with natural gas , gasoline and charge dilution, Fuel 304 (2021) 121438, https://doi.org/10.1016/j.fuel.2021.121438.
[6] A. Alper, Y. Do, Investigation of the effects of gasoline and CNG fuels on a dual sequential ignition engine at low and high load conditions, Fuel 232 (2018) 114–123, https://doi.org/10.1016/j.fuel.2018.05.156.
[7] R.S. Hosmath, N.R. Banapurmath, S. V Khandal, V.N. Gaitonde, Y. H. Basavarajappa, V.S. Yaliwal, Effect of compression ratio , CNG flow rate and injection timing on the performance of dual fuel engine operated on honge oil methyl ester (HOME) and compressed natural gas (CNG), Renew. Energy 93 (2016) 579–590, https://doi.org/10.1016/j.renene.2016.03.010.
[8] T. Wongwuttanasatian, S. Jankoom, K. Velmurugan, Experimental performance investigation of an electronic fuel injection-SI engine fuelled with HCNG (H2 + CNG) for cleaner transportation, Sustain. Energy Technol. Assessments 49 (2022) 101733, https://doi.org/10.1016/j.seta.2021.101733.
[9] R. Singh, L.M. Das, Performance and emission assessment of a multi- cylinder S . I engine using CNG & HCNG as fuels, Int. J. Hydrogen Energy 44 (2019) 21181–21192, https://doi.org/10.1016/j.ijhydene.2019.03.137.
[10] P. Lino, G. Maione, Accurate dynamic modeling of an electronically controlled CNG injection system, IFAC-PapersOnLine 49 (2016) 490–496, https://doi.org/10.1016/j.ifacol.-2016.08.072.
[11] S. Munahar, M. Setuyo, R.A. Brieghtera, M.M. Saudi, A. Ahmad, D. Yuvenda, Fuel control system on CNG fueled vehicles using machine learning: a case study on the downhill, Autom. Exp. 6 (2023) 173–187, https://doi.org/10.31603/ae.8107.
[12] S. Ryu, D. Kim, B. Lee, D. Han, I. Jung, J. Chung, Idle vibration reduction of a diesel Sport utility vehicle, Appl. Sci. 12 (2022), https://doi.org/10.3390/app12115448.
[13] V. Velmurugan, C. Naveen Kumar, V. Paramasivam, S. Thanikaikarasan, Prediction of noise, vibration and exhaust gas emission characteristics using palm oil in a four stroke diesel, Mater. Today Proc. 21 (2020) 896–901, https://doi.org/10.1016/j.matpr.2019.08.066.
[14] B. Ashok, A. Tamilvanan, R. Vignesh, P. Saiteja, P.V. Kumar, C. Nikhil, D. Nikhil, Engine vibration and noise characteristics of common rail direct injection engine fuelled with orange peel oil by response surface methodology based multi-objective optimization, Results Eng 20 (2023) 101406, https://doi.org/10.1016/j.rineng.2023.101406.
[15] J. Zhou, L. Zhou, F. Luo, Z. Zhou, Effect of injection parameters on vibration of high pressure common rail diesel engine for light vehicle at idle speed, J. Phys. Conf. Ser. 1549 (2020) 1–8, https://doi.org/10.1088/1742-6596/1549/4/042090.
[16] M.R. Reksoprodjo, W. Nirbito, Characteristics of vibration propagation on passenger car monocoque body structure at static small turbocharged diesel engine speed variation, J. Phys. Conf. Ser. 1519 (2020) 1–9, https://doi.org/10.1088/1742-6596/1519/1/012005.
[17] A. Khajehdezfuly, A.A. Shiraz, J. Sadeghi, Assessment of vibrations caused by simultaneous passage of road and railway vehicles, Appl. Acoust. 211 (2023) 109510, https://doi.org/10.1016/j.apacoust.2023.109510.
[18] S. Rana, Asaduzzaman, Vibration based pavement roughness monitoring system using vehicle dynamics and smartphone with estimated vehicle parameters, Results Eng 12 (2021) 100294, https://doi.org/10.1016/j.rineng.2021.100294.
[19] J. Hunicz, M.S. Geca, E. Ratajczyk, A. Mahmoudzadeh, M. Mikulski, An analytical approach to using the vibration signal to determine combustion characteristics of homogeneous charge compression ignition engines, SSRN Electron. J. 294 (2023), https://doi.org/10.2139/ssrn.4397080.
[20] N. Hashiguchi, J. Cao, Y. Lim, S. Kuroishi, Y. Miyazaki, S. Kitahara, S. Sengoku, K. Matsubayashi, K. Kodama, Psychological effects of heart rate and physical vibration on the operation of construction machines: experimental study, JMIR MHealth UHealth 9 (2021) 1–17, https://doi.org/10.2196/31637.
[21] J.M. Hooper, D. Williams, K. Roberts-Bee, A. McGordon, P. Whiffin, J. Marco, Defining a vibration test profile for assessing the durability of electric motorcycle battery assemblies, J. Power Sources 557 (2023) 232541, https://doi.org/10.1016/j.jpowsour.2022.232541.
[22] S. Chen, M. Hu, Active torsional vibration suppression of integrated electric drive system based on optimal harmonic current instruction analytic calculation method, Mech. Mach. Theor. 180 (2023) 110837, https://doi.org/10.1016/j.mechmachtheory.2022.105136.
[23] H. Zhang, L. Wang, A. Wang, Vibration response analysis of gas generator rotor system with squeeze film damper based on dynamic similarity, Results Eng (2023) 107386, https://doi.org/10.1016/j.rineng.2023.101618.
[24] R.C. Caryn, J.P. Dickey, Transmission of acceleration from a synchronous vibration exercise platform to the head during dynamic squats, Dose Response 17 (2019) 330–338, https://doi.org/10.1177/1559325819827467.
[25] O. Avci, O. Abdeljaber, S. Kiranyaz, M. Hussein, M. Gabbouj, D.J. Inman, A review of vibration-based damage detection in civil structures: from traditional methods to Machine Learning and Deep Learning applications, Mech. Syst. Signal Process. 147 (2021) 107077, https://doi.org/10.1016/j.ymssp.2020.107077.
[26] S. Munahar, M. Setiyo, M.M. Saudi, A. Ahmad, D. Yuvenda, Modelling fuel cut off controller on CNG engines using fuzzy logic: a prototype, Int. J. Adv. Sci. Eng. Inf. Technol. 12 (2022) 1857–1865, https://doi.org/10.18517/ijaseit.12.5.16849.
[27] MathWorks, Modeling engine timing using triggered subsystems, MathWorks (2021).Access August 2023, https://www.mathworks.com/help/simulink/slref/modeling-engine-timing-using-triggered-subsystems.html.
[28] J. Muir, D.P. Kiel, C.T. Rubin, Safety and severity of accelerations delivered from whole body vibration exercise devices to standing adults, J. Sci. Med. Sport 16 (2013) 526–531, https://doi.org/10.1016/j.jsams.2013.01.004.
[29] A.G. Ambeker, Mechanical Vibrations and Noise Engineering, Prentice Hall India, 2006. https://books.google.co.id/books?id=-ZtcUeV137EC&printsec=frontcover&redir_esc=y#v=onepage&q&f=false.
[30] Z. Ghemari, F. Chouaf, S. Saad, New formula for the piezoresistive accelerometer motion acceleration and experimental validation, J. Adv. Manuf. Syst. 16 (2017) 57–65, https://doi.org/10.1142/S0219686717500044.
[31] A. Rashid, O. Hasan, Formal analysis of continuous-time systems using Fourier transform, J. Symbolic Comput. 90 (2019) 65–88, https://doi.org/10.1016/j.jsc.2018.04.004.
[32] P. Liu, Time-frequency analysis of event-related potentials associated with the origin of the motor interference effect from dangerous objects, Brain Res. 1682 (2018) 44–53, https://doi.org/10.1016/j.brainres.2018.01.005.
[33] J. Zhang, N. Jiang, C. Zhou, K. Zhao, B. Zhu, Quantitative evaluation method of human comfort under the influence of blast vibration based on human physiological indexes and its application, Appl. Acoust. 202 (2023) 109175, https://doi.org/10.1016/j.apacoust.-2022.109175.
[34] Y. Liu, Y. Wang, Vibration suppression of a linear oscillator by a chain of nonlinear vibration absorbers with geometrically nonlinear damping, Commun. Nonlinear Sci. Numer. Simul. 118 (2023) 107016, https://doi.org/10.1016/j.cnsns.2022.107016.